https://doi.org/10.3311/PPci.42767

Periodica Polytechnica Civil Engineering

Effect of Curing Conditions on the Properties of Magnesium Phosphate Cement and its Bonding Properties with Cement Mortar

Yunpeng Xie[1], Junchang Li[1], Weihao Li[1], Xiuhao Li[1], Ke Chen[1], Chenyang Ma[1*]

[1] State Key Laboratory of Tunnel Engineering, School of Civil Engineering, Shandong University, 73 Jingshi Road, 250061, Jinan, China
[*] Corresponding author, e-mail: machenyang@sdu.edu.cn

Received: 08 November 2025, Accepted: 12 April 2026, Published online: 01 June 2026

Abstract

Magnesium phosphate cement (MPC) can be used as a rapid repair material due to its excellent mechanical properties and high bonding strength. However, the properties of MPC are significantly influenced by the environment but have been poorly studied in previous research. This paper researched the effects of four curing conditions on the properties and microstructures of hardened MPC, and the bonding mechanism between the MPC and OPC mortar was also investigated. The experimental results showed that water conditions decreased the mechanical strength and bonding strength compared to standard conditions, increasing the volume of large pores due to the dissolution of hydration products. Meanwhile, the phosphate hydrates were highly soluble in the alkaline solutions, leading to a significant increase in total porosity, but the compressive strength and bonding strength were not decreased due to the physical filling effect and chemical reaction of $Ca(OH)_2$. Additionally, the high temperature inhibited the hydration process of MPC, enhancing the decomposition of the main hydration product, and the bonding strength sharply decreased. Finally, the bonding mechanism between MPC and OPC included mechanical interlocking and chemical reactions. The former lost its effect in the heat due to the cracks and broken interfaces, and the latter was diminished in the wet environment for the phosphate was more likely to dissolve in the water instead of penetrating into the OPC phase. Therefore, the MPC is not suitable for wet environments and high-geothermal environments.

Keywords

magnesium phosphate cement, curing conditions, strength, microstructure, mechanism

1 Introduction

In recent years, tunnel development in China has accelerated in response to the growing traffic requirements [1]. During the progress of tunnel construction, concrete is normally intended as the support to stabilize the excavated tunnel, called the initial lining [2]. The secondary lining is installed as a remedial measure to enhance the stability and bearing performance of the tunnel [3–4]. This composite lining system offers advantages like structure strengthening, waterproofing, and so on. However, the time intervals between the installation of the double lining are uncertain in the field construction process. The gaps will appear between the initial and secondary lining due to the external loads, volume shrinkage, and other reasons, negatively affecting the integrity of the system and becoming a vital reason for the deterioration of lining concrete, water leakage, and other problems. Therefore, to ensure the stability and safety of the tunnel structure, the gaps need to be filled and repaired, and the selection of repair materials plays a key role.

MPC is a novel inorganic cementitious material, and the neutralization reaction occurs between dead-burnt MgO and acid phosphate [5]. Some literature showed that magnesium phosphate cement (MPC) exhibits numerous superior qualities compared to the OPC, including quick setting times, high early mechanical properties, minimal drying shrinkage, and strong bond properties, and it has been applied for the rapid repair of engineering [5–9]. However, the complex tunnel environment was affected by factors including water, pH, temperature, and so on, posing a challenge for the application of MPC. The gaps between the initial and secondary lining lead to the deterioration of concrete and water leakage, resulting in a wet environment of the tunnel. Additionally, the dissolution of concrete hydration products will increase the pH of water. At present, abundant studies have been conducted to research the water stability of MPC [10–14], and the degradation mechanisms have been revealed [12–14]. However, the research under alkaline environments has

Cite this article as: Xie, Y., Li, J., Li, W., Li, X., Chen, K., Ma, C. "Effect of Curing Conditions on the Properties of Magnesium Phosphate Cement and its Bonding Properties with Cement Mortar", Periodica Polytechnica Civil Engineering, 2026. https://doi.org/10.3311/PPci.42767

barely been investigated. Zhong et al. [15] researched the effect of alkaline solutions on the properties and microstructures of hardened MPC, presenting that the decreased properties were related to the pH. The high-alkaline solution triggered the lower strength, the higher porosity, and the loose microstructure. In addition, the temperature is an important factor in the characteristics of the MPC [16–17]. The struvite ($NH_4MgPO_4 \cdot 6H_2O$) would dehydrate to form the dittmarite ($NH_4MgPO_4 \cdot H_2O$) [16], and the NH_3 would be continuously released due to the decomposition of hydration products [18]. The high geothermal environment was inevitably encountered with the construction of tunnels in deep underground space, but few studies were concerned about the properties of MPC in slightly elevated temperatures. Xu et al. [17] found that the K-struvite ($KMgPO_4 \cdot 6H_2O$) progressively decomposed at 50 ℃, leading to decreased strength and volume shrinkage.

Now it is commonly acknowledged that, besides mechanical strength, other qualities of repair materials, such as bond strength and interfacial permeability, are equally essential to the success of the repair [19–21]. Some researchers believed that the MPC displays excellent bond characteristics under normal conditions, and it was characterized by high bond strength and minimal dry shrinkage [19]. Previous studies showed that the strong bond strength of MPC depended on the concrete substrate with suitable conditions, such as interfacial moisture, roughness, and concrete strength [22–23]. However, it is attributed that the decreased strength of MPC under water conditions leads to a decline or failure of interface adhesion [12]. Therefore, the bonding properties of MPC and OPC interacting with water need notice. Hitherto, few scholars have investigated this subject, but in most cases, they only focused on the bond strength under normal conditions. Therefore, when studying the bonding properties of MPC, it is necessary to make further research on the effect on the water environment. Additionally, the impact of high temperature and alkaline solution on the bonding properties was investigated, corresponding to the tunnel of high geothermal and groundwater with high pH, respectively, so it can provide effective guidance for the application of MPC in the tunnel field.

In this paper, four different curing conditions were set and the differences in mechanical strength were investigated. The flexural bonding strength was used to characterize the bonding properties between MPC and OPC. In addition, the microstructure of MPC under different curing conditions and the bonding mechanism of the interface between the MPC and OPC was analyzed by means of Mercury Intrusion Porosimetry (MIP), X-ray Diffraction (XRD), Scanning Electron microscope (SEM), and matched Energy Dispersive Spectrometer (EDS).

2 Materials and methods

2.1 Raw materials

Magnesium oxide (MgO, M), ammonium dihydrogen phosphate ($NH_4H_2PO_4$, ADP, P), and borax ($Na_2B_4O_7 \cdot 10H_2O$, B) were purchased from Guizhou Magnesium Phosphate Materials Co., Ltd. The MgO was the dead-burnt magnesium oxide under a 1700 ℃ calcination with a purity of 85%. The ADP and borax were all industrial-grade white crystalline powder, and their purity was 99%. Ordinary Portland Cement was used in this study, and it was provided by Shandong Zhucheng Jiuqi Building Materials Co., Ltd. The sand was purchased from Xiamen ISO Standard Sand Co., Ltd, and its particle diameter was less than 0.6 mm. Meanwhile, the chemical compositions of MgO and cement were shown in Table 1, and the particle size distributions were shown in Fig. 1.

2.2 Mix proportion

The mass ratio of M/P was fixed at 3.5 in this study, and the B/M was 10%. Meanwhile, the water was 0.16 of the solid mass. To precisely quantify the water content of the MPC, the crystalline water in the borax was considered in this study. The MgO, ADP, and borax were first mixed in proportion and stirred evenly, then the water was added and stirred for at least 3 min to prepare the MPC. The mortar was prepared with a cement/sand/water mass ratio of 1:3:0.5, the density was 2.135 g/cm^3 and the 28 d compressive strength was 40 MPa. The cement and sand were mixed firstly in a JJ-5 mixer for 30 s, then the water was added and stirred for another 120 s. The main properties of the MPC were shown in Table 2.

2.3 Curing condition

The properties of the specimens were determined by subjecting them to four different cueing conditions:

Table 1 Chemical compositions of the MgO and Cement

	CaO	SiO_2	Al_2O_3	Fe_2O_3	MgO	SO_3	K_2O	TiO_2	Na_2O	P_2O_5
MgO	4.133	8.044	0.773	1.121	84.969	0.027	0	0.066	0	0.867
Cement	56.090	23.117	8.987	4.899	2.815	2.448	0.779	0.591	0.148	0.126

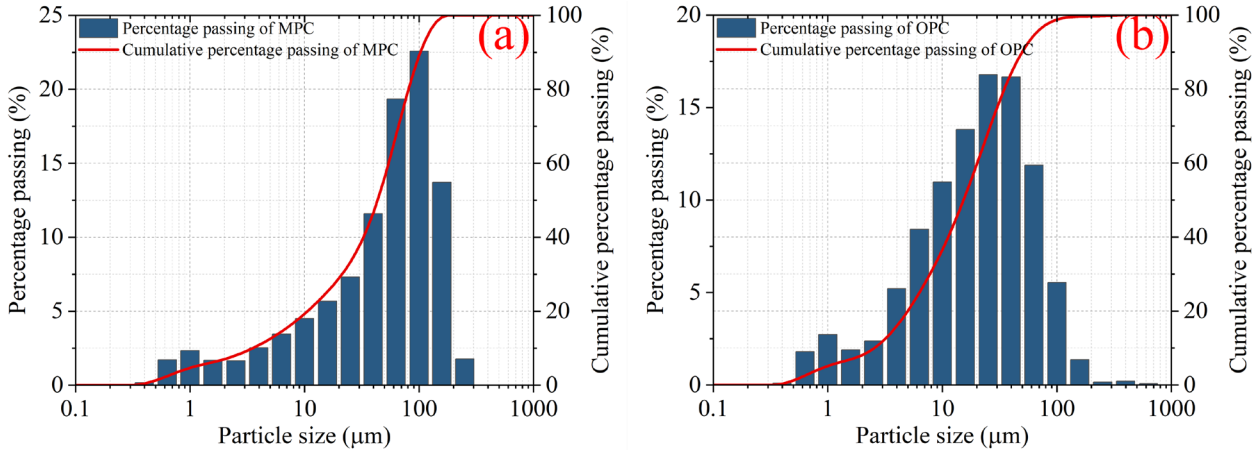

Fig. 1 The particle size distribution of MgO and cement: (a) MgO; (b) OPC

Table 2 The main properties of MPC

Property	Value
Fluidity	250 mm ± 5 mm
Setting time	10 min ± 0.5 min
Density	2.3 g/cm^3 ± 0.05 g/cm^3
Compressive strength (3h)	40 MPa ± 2 MPa
Compressive strength (28d)	70 MPa ± 5 MPa

- Curing condition 1, standard: after demolding in 3 d, the specimens were put into the constant temperature humidity chamber (20 ± 2 °C, relatively humidity ≥ 95%) until 28 d.
- Curing condition 2, water: after demolding in 3 d, the specimens were put into water (20 ± 2 °C) until 28 d (pH = 7).
- Curing condition 3, steam: after demolding in 3 d, the specimens were put into the high-temperature chamber (60 ± 2°C, relatively humidity ≥ 95%) until 28 d.
- Curing condition 4, alkaline: after demolding in 3 d, the specimens were put into the saturated $Ca(OH)_2$ solution (20 ± 2 °C) until 28 d (pH = 12.6).

To simulate the alkaline groundwater environment in tunnels, a saturated calcium hydroxide solution was prepared as the curing medium. The preparation method for the saturated calcium hydroxide aqueous solution was as follows: excess $Ca(OH)_2$ powder was added to deionized water at a room temperature of 20 °C. The mixture was continuously stirred for 30 min to ensure sufficient dispersion and dissolution and then left to stand for 24 h to allow the undissolved solids to settle. The supernatant was collected via filter paper filtration or centrifugation to obtain the saturated limewater. The main performance indicators of the saturated calcium hydroxide aqueous solution are shown in Table 3.

Table 3 Main properties of the saturated calcium hydroxide aqueous solution

Property	Value
Solubility at 20 °C	1.5 g/L
Saturated molar concentration	0.02 M
Saturated mass concentration	1.5 g/L
pH of saturated solution	12.6

The codes were used in this study to clearly illustrate the different specimens and curing conditions. For example, MPC-1 indicated the MPC is cured in the standard condition, while OPC-MPC-2 indicated the bonding specimens cured in the water.

2.4 Test program

2.4.1 Mechanical property

The MPC slurry was poured into the mold (40 mm × 40 mm × 160 mm), and the flexural strength was measured with three specimens. The compressive strength was tested using the two prisms after the flexural test. The mechanical properties were tested using an electronic universal testing machine, and the loading speed was 0.5 mm/min.

2.4.2 Bonding characteristic

The mold size of the bond strength was 40 mm × 40 mm × 160 mm, and the specimens were prepared in two steps. Firstly, the foams with a size of 40 mm × 40 mm × 80 mm were put into the molds, and the OPC mortar was poured into the remaining area. The foams were removed after 3 days, the interfaces of mortar were polished, and then the MPC slurry was poured. The specimens were demolded after 3 hours and put into four different curing conditions for bond strength measurement. The bond strength was measured using the flexural method and the

electronic universal testing machine at 28 d age. Meanwhile, the failure modes were recorded, and the microstructures of the bond interfaces between the MPC and OPC mortar were observed by SEM&EDS.

2.4.3 Pore structure

The small pieces (no more than 2 g for mass and 1 cm × 1 cm × 1 cm for volume) were used to measure the porosity and pore size distribution of the MPC specimens under different curing conditions by MIP (Micromeritics AutoPore V 9620 made in US) method. The maximum intrusion pressure was 30000 psi.

2.4.4 SEM&EDS analysis

The SEM&EDS analysis was performed to observe the microstructure of the materials. The pieces were polished by using the emery papers and then examined in an SEM (TESCAN MIRA LMS made in Czech) with the accelerating energy of 15 kV. Regional element analysis including spot and mapping was performed by matched EDS.

2.4.5 XRD analysis

The pieces were crushed into powder by agate mortar and then examined in an XRD (Bruker D8 Advance made in German). XRD analysis was conducted with a scanning rate from 5° to 90° at 2°/min, and the results were quantitatively analyzed by the Rietveld treatment.

2.4.6 Moisture content test

First, the specimens were taken out of the curing room, and the free water on their surfaces was quickly wiped off with a damp towel to achieve a saturated surface-dry (SSD) state. Subsequently, the mass of the specimen was immediately weighed using a balance and recorded as m_1. Then, the specimen with the initial mass was placed in an oven and dried at 80 °C for 24 h. After being removed and weighed, it was returned to the oven to dry for another 1 h and weighed again. If the mass difference between the two consecutive weighings did not exceed 0.1%, the specimen was considered to have reached a constant weight. This final mass was recorded as m_2. Finally, the moisture content, μ, was calculated using the following formula:

$$\mu = \frac{m_1 - m_2}{m_2} \times 100\%$$

3 Results

3.1 Flexural strength and compressive strength

As shown in Fig. 2, the flexural strengths of MPC-1, MPC-2, MPC-3, and MPC-4 were 10.721 MPa, 10.632 MPa, 7.597 MPa, and 15.158 MPa, while the compressive strengths were 64.552 MPa, 58.632 MPa, 74.377 MPa, and 61.014 MPa, respectively. It could be seen that the strength of MPC under the standard condition was slightly higher than that of the water condition, and this was similar to the previous study [11, 24]. It is attributed to the dissolution of the hydration product [12]. Partial ADP was unreacted during the hydration process and was dissolved in the water at this time. So, the pH of the curing water decreased and then caused the further dissolution of the phosphate hydrates, leading to the decline of the strength [13, 25–26]. Note that the difference between the two values was not significantly obvious, while nearly 20% in other literature, and it is guessed to the high M/P ratio and the adequate chemical reaction degree [27].

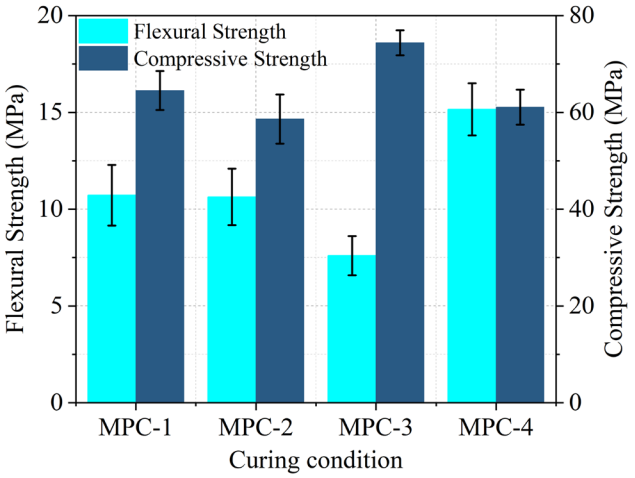

Fig. 2 The flexural strength and compressive strength of MPC under various conditions

A similar theory could be used to explain the changed strength of MPC-4. When soaked in the alkaline solution, the unreacted ADP was dissolved but had a rare effect on the pH of the curing solution. However, the high pH would also increase the solubility of hydration products and lead to a decrease in compressive strength [28]. In the previous study, the compressive strength of MPC cured in the low-alkalinity solution (pH = 12, NaOH) continuously increased at 28 d age, and there were no significant differences compared to the water condition [15]. Moreover, the $Ca(OH)_2$ in the alkaline solution may penetrate into the MPC, and the volumes of big pores were declared by the physical filling effect or chemical reaction. This was proved by the MIP results and SEM micromorphology in Section 4.

For MPC-3, the mechanical strengths showed a different trend, with the lowest flexural strength but the highest compressive strength. As reported in the literature, the compressive strength would be improved, as long as the curing temperature was below 70 °C [16]. As for the

flexural strength, it was guessed to the water evaporation due to the increased temperature. The flexibility of the specimens was reduced, resulting in a decrease in flexural strength. Meanwhile, this effect of flexibility had little impact on the compressive strength, so the mechanical strengths exhibited the opposite results.

In the 60 °C environment, struvite, the main hydration product of MPC, partially dehydrated and transformed into dittmarite, which contains less crystal water. As shown in Table 4, the moisture content of the MPC-3 group decreased by approximately 33% compared to the standard group, indicating a significant loss of bound water within the structure. Although the external humidity was 95%, the temperature of 60 °C accelerated the migration and consumption of moisture inside the MPC. The underlying reason for this phenomenon is that the release of water from the crystal lattice and its subsequent redistribution induced severe volume shrinkage at the microscopic level, generating invisible micro-cracks. This ultimately weakened the effectiveness of mechanical interlocking and chemical bonding, thereby leading to a drastic decline in both bonding strength and flexural strength.

3.2 Bonding characteristics

Fig. 3 showed the effect of curing conditions on the bonding strength between the MPC and OPC mortar. The specimens cured in the standard conditions and alkaline solution conditions showed high bonding strength. When the bonding specimens cure in water conditions, the strength was 3.048 MPa, nearly 2 MPa lower than that of standard conditions. This indicated that the hydration products would dissolve in the water and decrease the bonding strength [12, 26]. For OPC-MPC-4, a similar effect occurred in the MPC phase. However, the alkaline solution would enhance the secondary hydration of unreacted cement particles in the OPC phase [29–30], and the $Ca(OH)_2$ in the solution was penetrated into the interface. These effects improved the compactness of the interface, thus increasing the bonding strength.

For the results of OPC-MPC-3, it could be seen that the high temperature sharply decreased the bonding strength. It was mainly attributed to the loose interface due to the dry shrinkage. In the OPC phase, the C-S-H gel would lose crystal water [31–33] and the ettringite began to decompose in the high temperatures [33–34], leading to the loose matrix and volume shrinkage. Meanwhile, the main hydration product in the MPC phase, struvite, would also lose crystal water [16]. The combined effect of these two factors led to a significant reduction in bonding strength.

Table 4 Apparent moisture content of the specimens before and after fracture

Group	Apparent moisture content before fracture (%)	Internal moisture content after fracture (%)
MPC-1	12.5	11.8
MPC-2	14.2	13.5
MPC-3	8.4	7.6
MPC-4	13.8	13.2

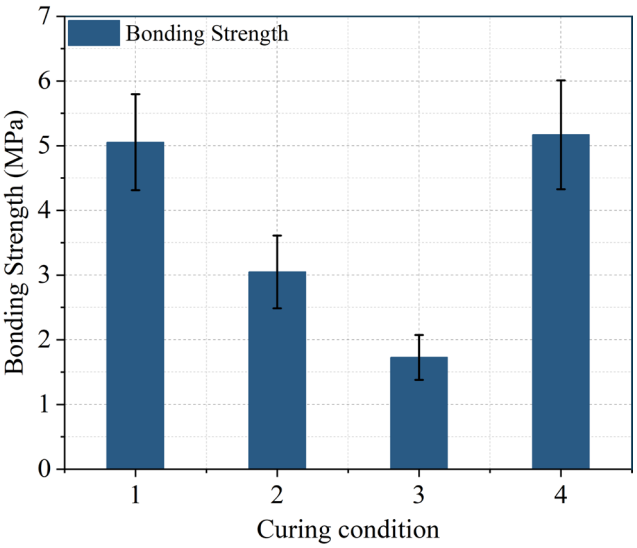

Fig. 3 The bonding strength of OPC-MPC under various conditions

It has been proven that the failure modes could be used to judge the quality of the bonding characteristics [19]. The failure of the bonding specimens had been summarized in three modes based on the failure positions: MPC, OPC, or interface [19, 35]. In this paper, the bonding specimens whatever curing conditions tend to an interfacial failure combined with partial OPC mortar. This phenomenon illustrated that the MPC had a high adhesive performance for OPC mortar, and it could be used for the repair of concrete.

4 Microstructure

4.1 Pore structure

Consistent with Fig. 3, Fig. 4 shows dense, tightly integrated MPC-OPC interfaces for MPC-1 and MPC-4. Conversely, MPC-2 exhibits pores and looseness, whilst MPC-3 displays cracks and shrinkage gaps.

Fig. 5 reported the porosity and pore volume distribution of MPC specimens. Compared to that cured in the standard conditions, the specimens cured in other conditions exhibited higher porosity. This illustrated the specimens in standard conditions contained relatively dense microstructure, causing a high compressive strength. For MPC-2, the pore volumes of any phase were all increased compared to MPC-1. It was attributed to the leaching effect of unreacted ADP during the water curing, and it could yield an open connect

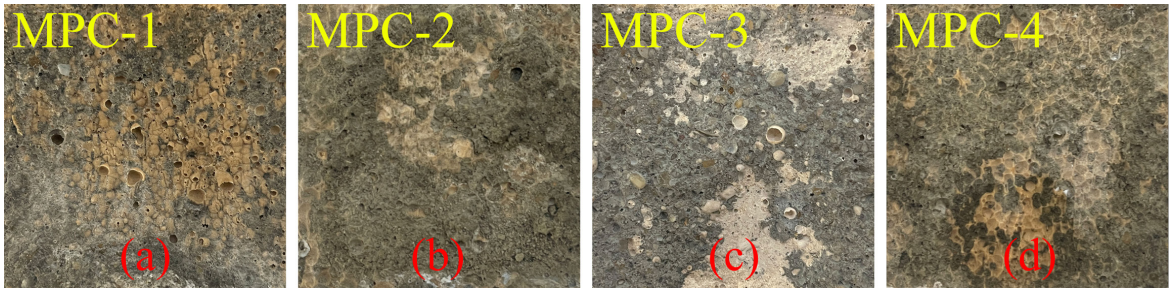

Fig. 4 The morphology of bonding interfaces: (a) MPC-1; (b) MPC-2; (c) MPC-3; (d) MPC-4

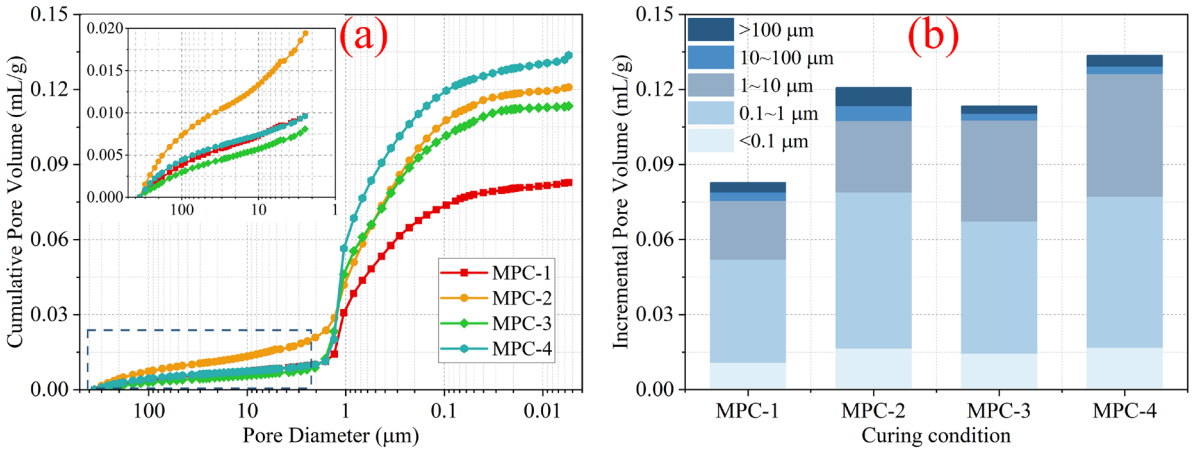

Fig. 5 The pore structure of MPC under various conditions: (a) Cumulative pore volume; (b) Incremental pore volume

porosity [36–37]. Moreover, the reaction product struvite would be dissolved and hence led to a loose microstructure.

The MPC-4 exhibited the maximum porosity in four curing conditions. Compared to MPC-2, it could be seen that the volume of tiny pores (< 1 μm) was similar. Moreover, the pores with a diameter of 1~10 μm were improved, and this was probably due to the improved dissolution of struvite in the alkaline solutions [28]. However, the volume of large pores (> 10 μm) was reduced. It was guessed that the physical filling effect and chemical reaction occurred between $Ca(OH)_2$ and MPC, thus decreasing the volume of big pores.

For MPC-3, the specimens cured in the high-temperature environment showed a different pore characterization. Compared to MPC-1, the total porosity was increased. In detail, the pores with a diameter < 10 μm were increased, while those > 10 μm were reduced. This could be used to explain the change in compressive strength. In reference to the relationship between compressive strength and pore structure of OPC materials, not only the total porosity but the volume of large pores exhibited a significant effect on the strength [38–39]. Therefore, the MPC-3 showed the highest compressive strength, while the MPC-2 showed the lowest one.

4.2 Hydration products

Fig. 6(a) showed the XRD patterns of specimens under different curing conditions and the Rietveld method was used to quantitatively analyze the proportion of mineral phases (Fig. 6(b)). It could be seen that MgO, struvite, and dittmarite were the main mineral phases in the specimens. Apart from the main phases, other phases were found maybe including borax and crystals formed by the impurities in the MgO. A large proportion of dittmarite was found in the hardened MPC, and it was attributed to the rapid hydration. It had been confirmed that the type of mineral phases was related to the hydration temperature due to the intense exothermal release in the hydration process, and the high temperatures inside the hardened MPC would enhance the decomposition of struvite for losing five water molecules to form the dittmarite [16]. Therefore, the struvite and dittmarite could exist together in the specimens.

As shown in Fig. 6, the different curing conditions had little effect on the mineral phases, while the identified amounts were significantly influenced. It could be seen that the MPC-1 had the most sufficient hydration reaction for its lowest amount of MgO and the highest amount of phosphate hydrates (struvite and dittmarite). For MPC-2, when the hardened MPC was immersed in water at an early age, partial hydration products would be dissolved into the

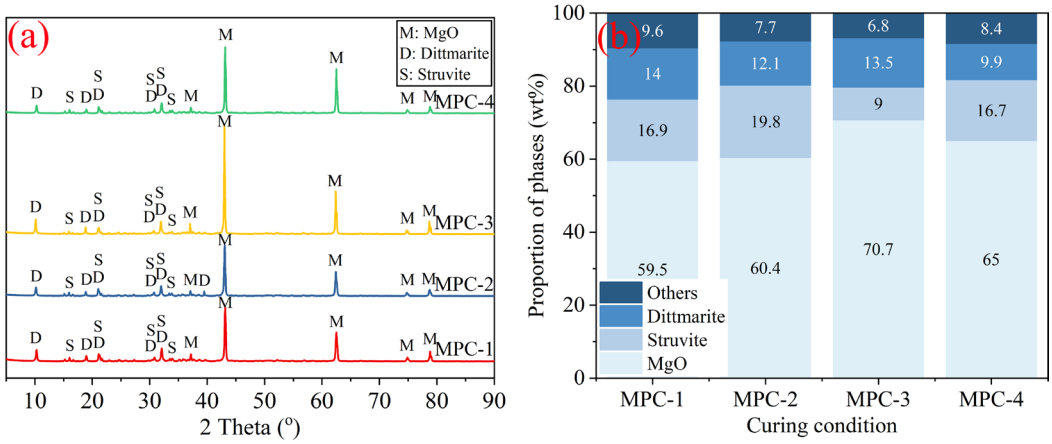

Fig. 6 Phase composition of MPC under different curing conditions: (a) XRD patterns; (b) quantitative phase proportions.

water, leading to a decreased amount of phosphate hydrates. When the specimens were immersed in the alkaline solution, the solubility of the products was further increased, resulting in the maximum porosity [28]. $Ca(OH)_2$ crystal was not examined in the XRD analysis due to the relatively small content, but it was found in the SEM images (Fig. 7(g)). Moreover, although there was no clear evidence observed in the XRD patterns, it was guessed that some other products might have been formed by the reaction between $Ca(OH)_2$ and phosphate to fill the large pores due to their amorphous nature.

For MPC-3, the proportion of MgO reached the maximum in the hardened MPC, illustrating that the high-temperature steam curing conditions would inhibit the hydration reaction. This seemed to contradict the change in compressive strength. It was worth noting that the micromorphology was affected by the high temperatures such as increased size, leading to the transformation and development towards the ceramic matrix [40–41] (Fig. 7(f)). This might the reason for the decreased large pores and increased compressive strength. Meanwhile, the long-term curing at 60°C would cause partial dehydration of struvite to dittmarite at 28 d age[16]. Therefore, the amount of dittmarite was not reduced while the amount of struvite was in substantial reduction.

4.3 Micromorphology

4.3.1 Micromorphology in MPC

Fig. 7 showed the microstructures of MPC under different curing conditions at 28d age. It could be seen that the MgO was tightly combined with the phosphate hydrates [42]. The hydration products were recognized as binders and could bond the unreacted MgO to form a dense microstructure, enhancing the early strength gains [18, 43]. Moreover, the hydration products exhibited various morphologies [16]. Some crystals seemed like block or tabular plates, and they were typical morphology of struvite [16, 44]. Other perfect microstructures presented a flower-like shape with many sheet layers, and they were dittmarite formed by the dehydration of struvite. Similar structures of struvite and dittmarite were observed in the previous studies [5, 18].

Compared to MPC-1, the microstructure of MPC-3 exhibited a ceramic matrix under the effect of high temperatures [40]. Some micro-cracks were observed in the matrix, and this was attributed to the continuous dehydration and decomposition of struvite in the heat [16, 19]. Meanwhile, previous studies showed that the NH_3 would be released when the temperature was 50 °C [18]. These structural changes increased the internal stresses of the matrix, leading to the generation of micro-cracks. In addition, the hydration products were deposited randomly and gathered loosely in the high curing temperatures, increasing the early strength due to the rapid hydration but decreasing the long-term strength as the irregular crystal microstructures [17].

When the hardened MPC was immersed in the water, the phosphate hydrates were dissolved, and the decreased pH of water enhanced the further dissolution of MgO [12–13]. This expressed the loose microstructure within the matrix (Fig. 7(d)), which decreased the compressive strength and increased the porosity [26]. Furthermore, it was proven that the hydration products exhibited greater solubility in the alkaline solutions, enhancing the further increase of porosity. However, some $Ca(OH)_2$ crystals were observed in the hardened MPC (Fig. 7(g)), illustrating $Ca(OH)_2$ could decrease the volume of large pores through the pore-filling effect.

As shown in Fig. 8, except for the obvious $Ca(OH)_2$ crystals, the calcium element also aggregated in the other regions. These products were not observed in the XRD analysis and were considered as the amorphous phases. The formation of these phases could partially compensate for the generation of large pores due to the increased dissolution of hydration

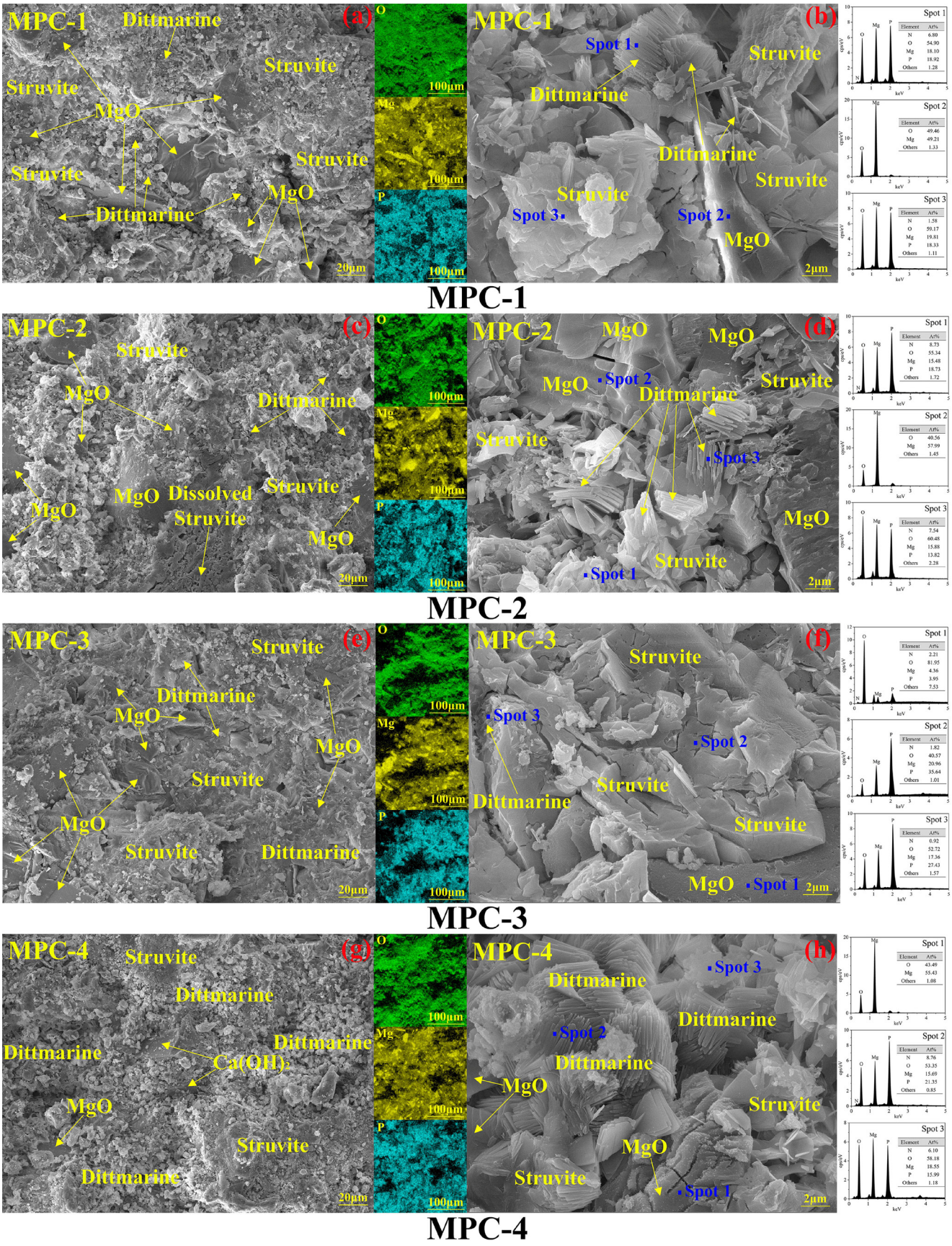

Fig. 7 SEM morphologies of hardened MPC at 28 d age: (a) overall view of MPC-1; (b) local detail of MPC-1; (c) overall view of MPC-2; (d) local detail of MPC-2; (e) overall view of MPC-3; (f) local detail of MPC-3; (g) overall view of MPC-4; (h) local detail of MPC-4

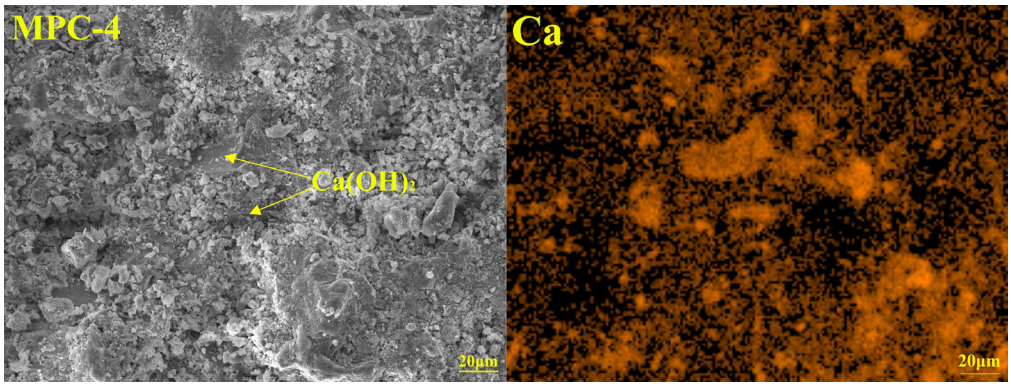

Fig. 8 The mapping results of the Ca element in MPC-4

products in the alkaline solutions. This might be the main reason for the improved compressive strength in MPC-4.

4.3.2 Micromorphology in the bonding interfac

Fig. 9 showed the microstructures of MPC and OPC bonding interfaces under different curing conditions at 28 d age, and the distribution of five elements (O, Si, Ca, Mg, and P) was detected by matched EDS. From the SEM images, it could be seen that the MPC phase and OPC phase were closely connected due to the strong physical effect, making the interfaces difficult to identify [19]. The MPC and OPC could be distinguished by the distribution of Mg and P, Ca and Si, respectively, and various hydration products were observed. Except for the mechanical effect, chemical interactions were also found in the interfaces [45, 46]. It could be observed that the EDS mapping image of element P exhibited an obvious integration into the OPC mortar phase, demonstrating the penetration of phosphate. The dissolution of phosphate would create an acidic environment in the interfacial zones, resulting in the erosion of OPC mortar. This enhanced the generation of micro-cracks in the OPC phases and benefited the penetration of element P. In previous studies, the phosphate in the OPC phases could react with the hydration products to form the secondary phosphate phase [46]. Therefore, it could be seen that the hydration products in OPC phases contained element P (Fig. 9 and Fig. 10). Moreover, due to the excellent

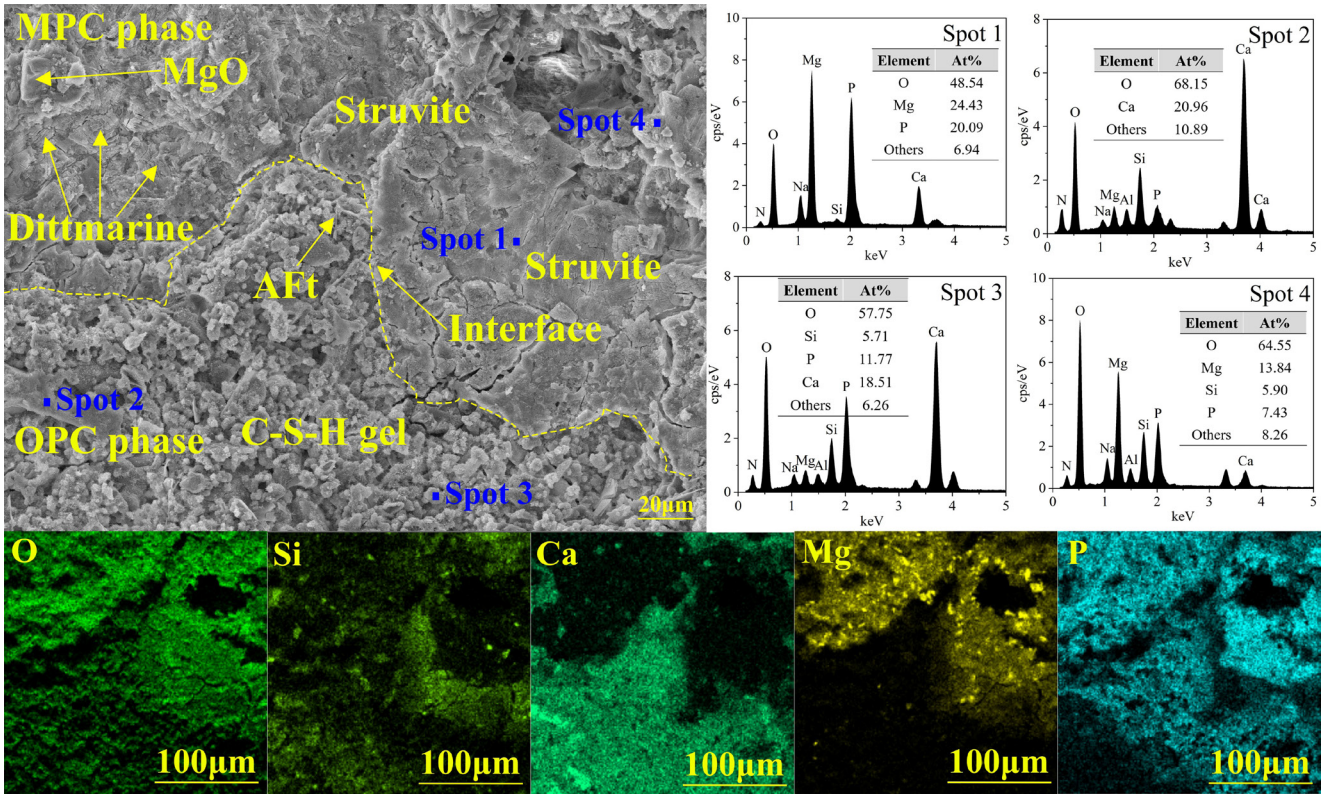

Fig. 9 SEM morphology of the bonding interface between MPC and OPC at 28 d age for OPC-MPC-1

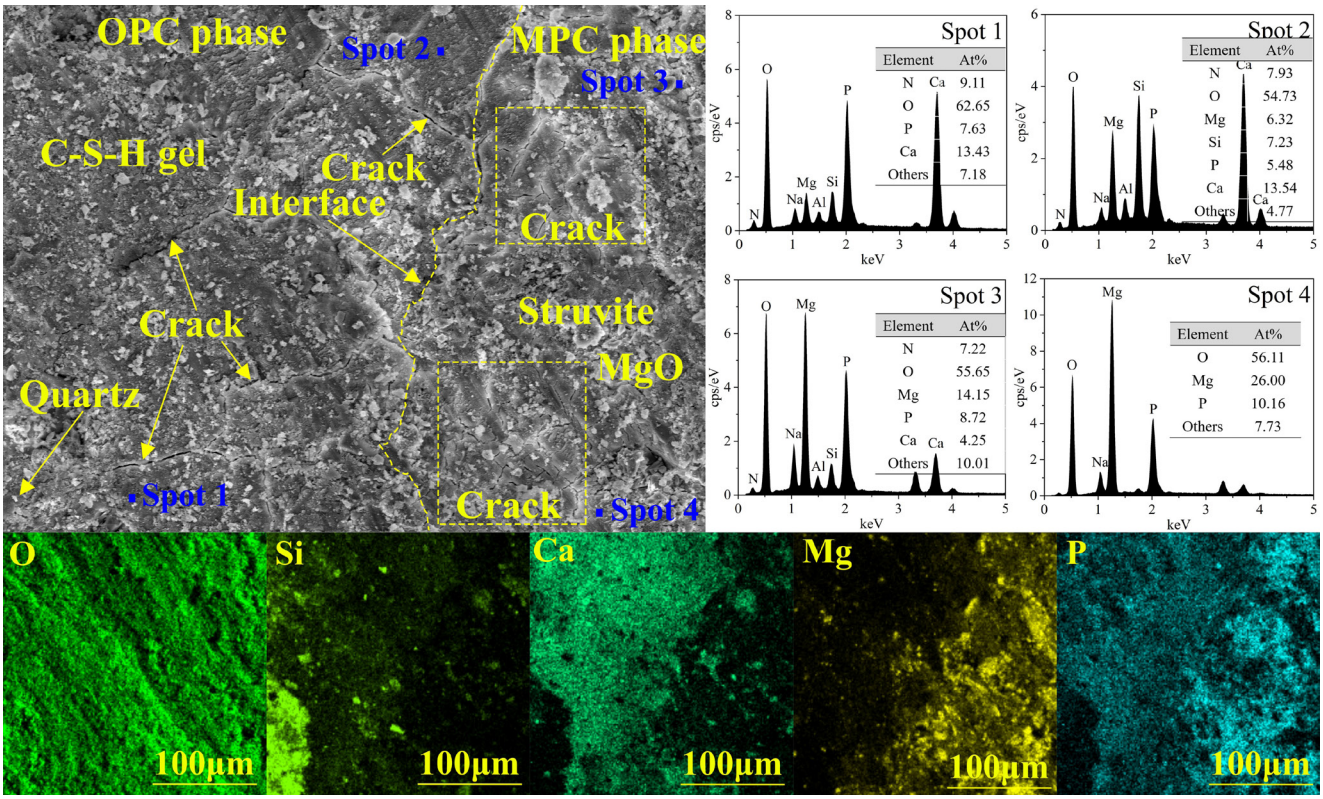

Fig. 10 SEM morphology of the bonding interface between MPC and OPC at 28 d age for OPC-MPC-3

workability and low viscosity at an early age, the MPC slurry could partially fill the cracks and create a mechanical link with the OPC phase in the hardened state [19, 47].

The brightness of EDS images was used to represent the concretion of chemical elements. For comparison, the brightness of element P in the OPC phase in OPC-MPC-1 and OPC-MPC-3 was larger than that in OPC-MPC-2 and OPC-MPC-4, indicating that the effect of chemical interactions became weak in the water or alkaline solution. When the bonding specimens were immersed in the water or alkaline solution, the dissolved phosphate was more likely to be lost to water, rather than penetrated into the OPC phase. On the contrary, the results of EDS mapping showed that the elemental composition of MPC hydrated phases in the interfacial zones contained O, Mg, and P as well as a minor amount of Ca, and Si. The secondary hydration of the OPC phase was produced in the water or alkaline solution, but the struvite and dittmarite would be dissolved, causing a loose microstructure. The products could fill the defects, like micro-cracks and pores, so elements Ca and Si were found in the MPC phase. An amount of element Ca (At% = 14.38%) was observed in spot 4 of OPC-MPC-2 (Fig. 11), illustrating that the calcium hydrogen phosphate or calcium phosphate might be formed. Similarly, magnesia silicate was found in the OPC-MPC-4 (Fig. 12), indicating that the penetration of element Si had occurred.

For OPC-MPC-3, a large number of micro-cracks were observed in whatever MPC phase or OPC phase. It was attributed to the effect of high temperatures on the morphology and mineral phase composition of hydration products. The C-S-H gels would lose the chemical-bound water and the ettringite would decompose in the heat [31–34]. As mentioned above, the struvite would be dehydrated to form the dittmarite under high temperatures, and the phosphate hydrates could release the NH_3, causing huge damage to the compactness of the matrix [16, 18]. Meanwhile, the changes in mineral phases were the vital factors of the volume shrinkage, causing a loose interface and a significant decrease in bonding strength.

5 Discussion

5.1 Mechanism of curing conditions on the MPC

Some literature had illustrated the reaction mechanism of MPC under water curing conditions [12, 25]. Water could penetrate into the matrix of MPC through the pores and micro-cracks, then the unreacted phosphate was dissolved. So the pH of the curing water decreased and then caused the further dissolution of the hydration products.

The alkaline solution would increase the solubility of hydration products, and this was identical to the previous study [15]. However, in this paper, the compressive strength did not decrease as mentioned in the literature, and this was

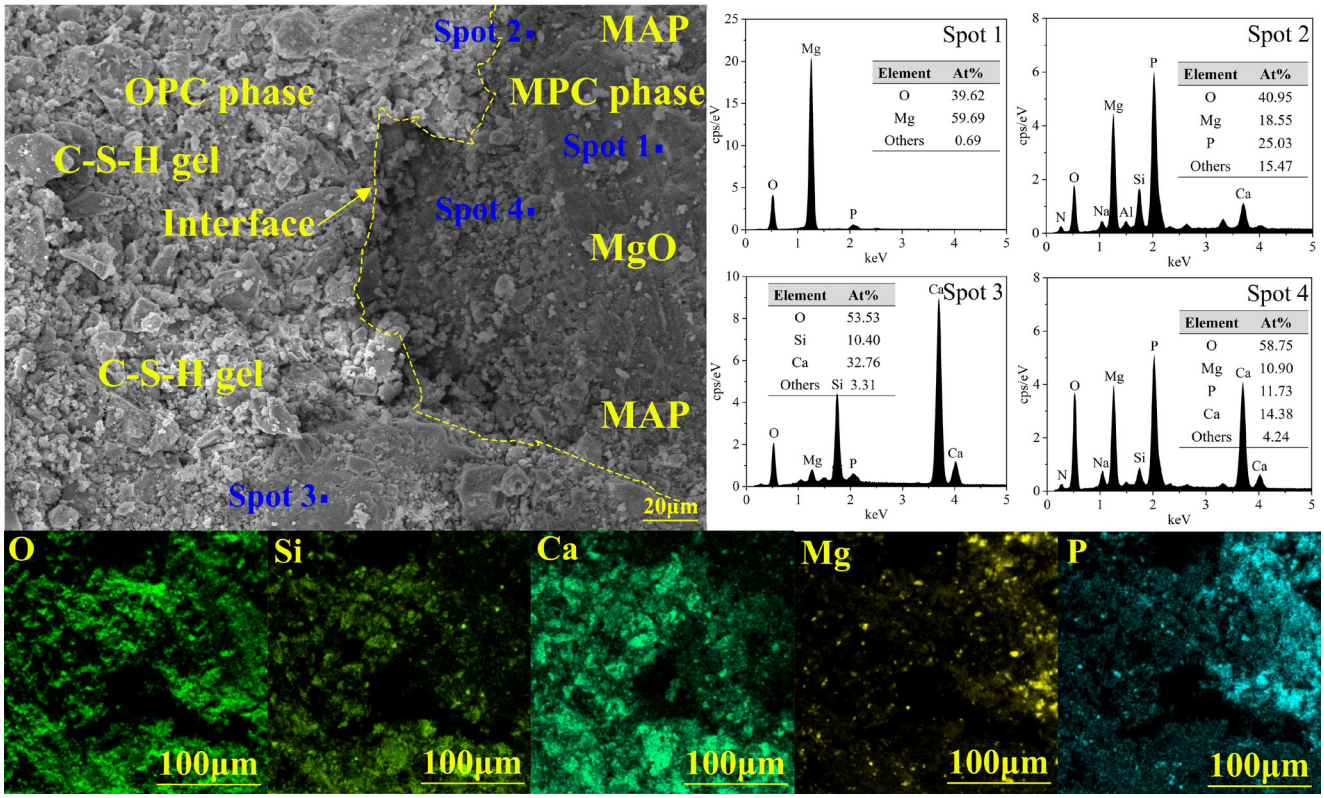

Fig. 11 SEM morphology of the bonding interface between MPC and OPC at 28 d age for OPC-MPC-2

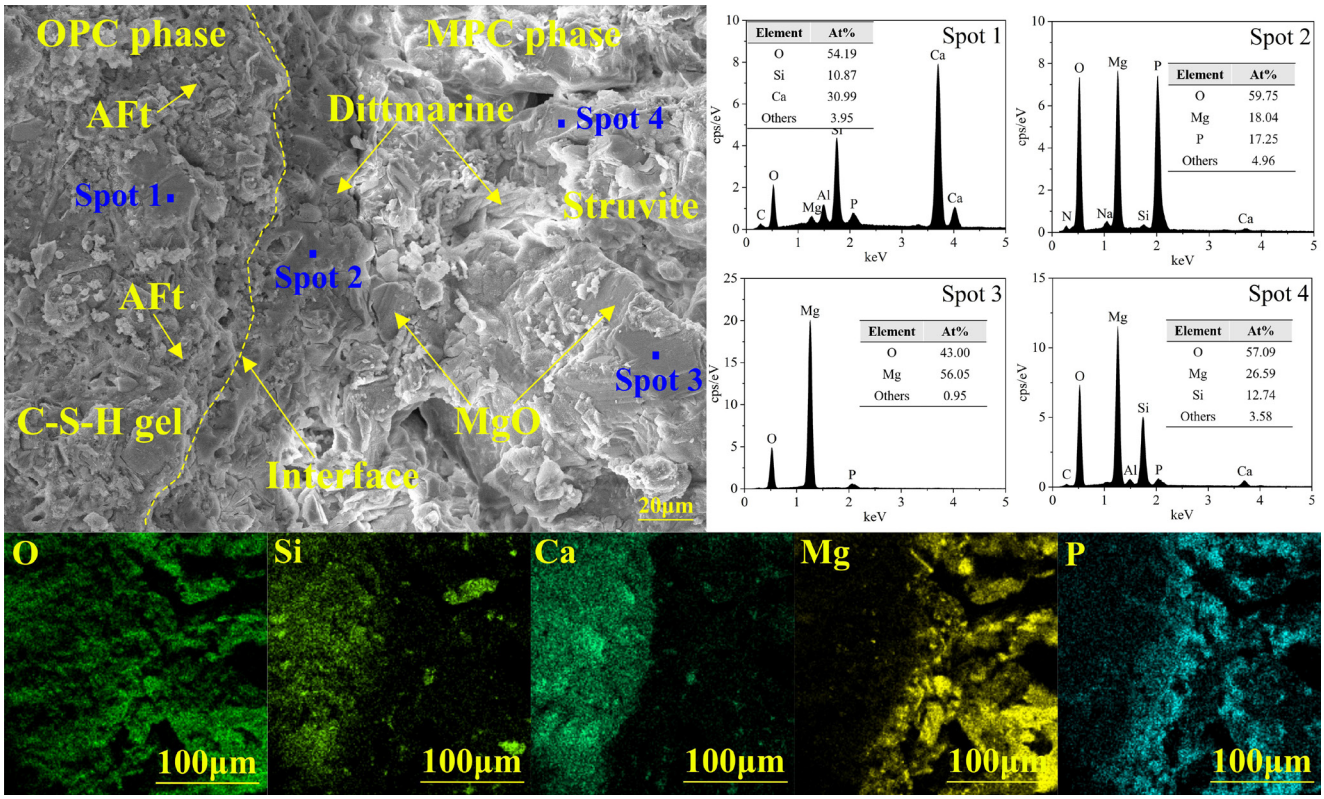

Fig. 12 SEM morphology of the bonding interface between MPC and OPC at 28 d age for OPC-MPC-4

attributed to the different alkaline solutions. In the tunnel, the alkaline water environment was mainly caused by the dissolution of the hydration products of concrete. Therefore, $Ca(OH)_2$ was more suitable in this study rather than NaOH. $Ca(OH)_2$ could fill partial pores through the micro-aggregated effect and block the water penetration into the matrix.

Meanwhile, $Ca(OH)_2$ could react with the phosphate hydrates to form some amorphous products. This could improve the density and compactness of the matrix, enhancing the compressive strength compared to water conditions.

Hitherto, few scholars have investigated the long-term high-temperature steam conditions on the properties of MPC. MPC has an intense hydration reaction, large hydration heat, and a large release of H_2, NH_3, and water vapor, causing a porous microstructure. This phenomenon was exacerbated when the hardened MPC was placed in a high-temperature environment [17]. Meanwhile, the gases escaped rapidly at an early age, leading to more pores in the matrix (Fig. 5). The hydration products were heterogeneously distributed and the microstructure exhibited much coarser. Furthermore, the loss of free water inhibited the further hydration of MPC (Fig. 6(b)), and the struvite was dehydrated to form the dittmarite in the heat. These had an impact on the microstructure and ultimately negated the long-term compressive strength.

5.2 Bonding mechanism of curing conditions on the MPC-OPC

The bonding mechanism of the MPC phase and the OPC phase was a synergistic effect of mechanical effect and chemical reaction in the interfacial zone [19, 47], as shown in Fig. 13. Firstly, the dissolution of phosphate created an acidic environment, enhancing the generation of more pores and cracks in the interface when contacted the surface of OPC mortar. Then some ions penetrated into the interior of the OPC phase and had a chemical reaction with calcium hydroxide or other hydration products, contributing to an excellent interfacial bond. Meanwhile, though the surface of the OPC mortar was polished to smooth, it became slightly rough after the erosion of acidic solutions (Fig. 4). The MPC slurry had low viscosity and excellent fluidity, so it could enter the OPC phase through the defects in the surface [45–46]. As a result, it successfully created a strong mechanical bond when the MPC slurry was solidified.

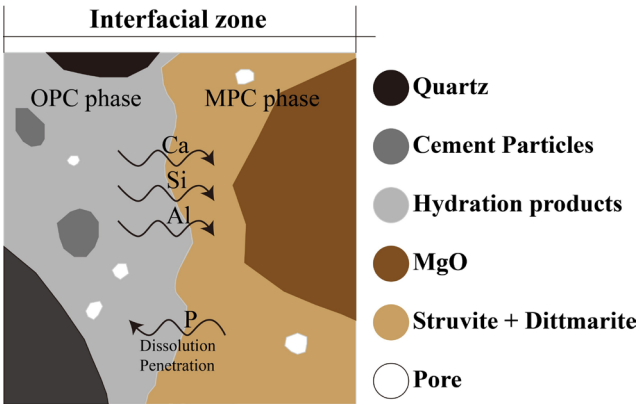

Fig. 13 The interfacial zone between the MPC phase and the OPC phase

When the hardened MPC was cured in the water or alkaline solutions, the penetration of phosphate became weak (Fig. 9). The dissolved phosphate was more likely to be lost to water, rather than penetrated into the OPC phase. The phosphate hydrates were easy to dissolve in the water, resulting in a loose interface and a decline of interfacial adhesion. On the other hand, due to the secondary hydration reaction of the OPC phase when in water or alkaline solution, the element Ca, Si, and unmarked Al reversely penetrated into the MPC phase. Except for the calcium hydrogen phosphate or magnesia silicate crystal, a large amount of amorphous material was formed. These products fill the interfacial zone between the MPC and OPC, improving the compactness and forming a dense bond interface. This partially compensated for the reduced bonding strength, especially for that cured in alkaline solutions (Fig. 3).

A large amount of element P penetrated into the OPC phase in the high-temperature environment (Fig. 10), creating a possibility for a chemical reaction in the interfacial zone. However, the broken interface under high temperatures rendered this effect ineffective. The interlacing cracks were generated and extended in the heat, breaking the mechanical interlocks between the OPC and MPC, so the bonding strength was significantly decreased. Therefore, the MPC was not suitable for the high geothermal tunnels.

6 Conclusion

The present study is concerned with the mechanical properties and microstructure of the hardened MPC and the bonding strength and micro-characterization between MPC and OPC mortar under different curing conditions. Based on the results and discussion, the conclusions can be summarized as follows:

1. The hardened MPC cured in standard conditions exhibits excellent compressive strength and bonding properties with OPC mortar. MPC -1 has the minimum porosity and the maximum hydration degree. The interface of OPC-MPC-1 shows a dense microstructure, expressing the high bonding strength at a macro level.
2. The water curing condition decreases the compressive strength and bonding strength. For MPC-2, the volume of large pores is significantly increased due to the dissolution of unreacted phosphate and hydration products. For OPC-MPC-2, the interface presents a loose structure thus decreasing the bonding strength.

3. The high-temperature steam curing conditions display the minimum flexural strength and the maximum compressive strength, and the bonding strength is the minimum. The hydration reaction is inhibited in the heat, and the amount of struvite decreases due to dehydration to form dittmarite. High-temperature environment enhances the inhomogeneous distribution of hydration products and the generation of cracks, leading to a broken microstructure.
4. When the specimens are immersed in the alkaline solutions, the compressive strength and bonding strength are all increased compared to the water condition. Although the total porosity is the highest due to the increased dissolution of hydration products in the alkaline solution, the volume of large pores decreases for the physical filling effect and chemical reaction of calcium hydroxide. Some crystals or amorphous phases are formed in the interfacial zones, thus improving the bonding properties.

Acknowledgments

This work was supported by the China Postdoctoral Science Foundation General Fund (2024M761809), the Postdoctoral Innovation Talent Support Program (BX20240209), Coal Mine Back-filling Mining National Engineering Research Center Innovation Project of Shandong Energy Group (SDEGIF-CT202504).

References

[1] Liu, D., Shang, Q., Li, M., Zuo, J., Gao, Y., Xu, F. "Cracking behaviour of tunnel lining under bias pressure strengthened using FRP Grid-PCM method", Tunnelling and Underground Space Technology, 123, 104436, 2022. https://doi.org/10.1016/j.tust.2022.104436

[2] Wang, X., Fan, F., Lai, J., Xie, Y. "Steel fiber reinforced concrete: A review of its material properties and usage in tunnel lining", Structures, 34, pp. 1080–1098, 2021. https://doi.org/10.1016/j.istruc.2021.07.086

[3] Chen, Q. J., Wang, J. C., Huang, W. M., Yang, Z. X., Xu, R. Q. "Analytical solution for a jointed shield tunnel lining reinforced by secondary linings", International Journal of Mechanical Sciences, 185, 105813, 2020. https://doi.org/10.1016/j.ijmecsci.2020.105813

[4] Wang, S., Jian, Y., Lu, X., Ruan, L., Dong, W., Feng, K. "Study on load distribution characteristics of secondary lining of shield under different construction time", Tunnelling and Underground Space Technology, 89, pp. 25–37, 2019. https://doi.org/10.1016/j.tust.2019.03.010

[5] Shi, J., Zhao, J., Chen, H., Hou, P., Kawashima, S., Qin, J., Zhou, X., Qian, J., Cheng, X. "Sulfuric acid-resistance performances of magnesium phosphate cements: Macro-properties, mineralogy and microstructure evolutions", Cement and Concrete Research, 157, 106830, 2022. https://doi.org/10.1016/j.cemconres.2022.106830

[6] Zhang, M., Zhang, Q., Pei, Y., Zhang, H., Chen, Z., Li, Y., Wang, K., Zhang, L., You, C., Skoczylas, F. "Injectability analysis of seawater-mixed magnesium phosphate cement slurry applied to a sand layer", Construction and Building Materials, 359, 129538, 2022. https://doi.org/10.1016/j.conbuildmat.2022.129538

[7] Qiao, F., Chau, C. K., Li, Z. "Property evaluation of magnesium phosphate cement mortar as patch repair material", Construction and Building Materials, 24(5), pp. 695–700, 2010. https://doi.org/10.1016/j.conbuildmat.2009.10.039

[8] Xu, B., Winnefeld, F., Kaufmann, J., Lothenbach, B. "Influence of magnesium-to-phosphate ratio and water-to-cement ratio on hydration and properties of magnesium potassium phosphate cements", Cement and Concrete Research, 123, 105781, 2019. https://doi.org/10.1016/j.cemconres.2019.105781

[9] Xu, B., Ma, H., Shao, H., Li, Z., Lothenbach, B. "Influence of fly ash on compressive strength and micro-characteristics of magnesium potassium phosphate cement mortars", Cement and Concrete Research, 99, pp. 86–94, 2017. https://doi.org/10.1016/j.cemconres.2017.05.008

[10] Shi, C., Yang, J., Yang, N., Chang, Y. "Effect of waterglass on water stability of potassium magnesium phosphate cement paste", Cement and Concrete Composites, 53, pp. 83–87, 2014. https://doi.org/10.1016/j.cemconcomp.2014.03.012

[11] Feng, H., Liang, J., Pang, Y., Zhao, X., Wang, Y., Sheikh, S. A. "Effects of the fly ash and water glass on the mechanical properties and water stability of the high ductile magnesium phosphate cement-based composite", Construction and Building Materials, 333, 127395, 2022. https://doi.org/10.1016/j.conbuildmat.2022.127395

[12] Feng, H., Zhao, X., Li, L., Zhao, X., Gao, D. "Water stability of bonding properties between nano-Fe_2O_3-modified magnesium-phosphate-cement mortar and steel fibre", Construction and Building Materials, 291, 123316, 2021. https://doi.org/10.1016/j.conbuildmat.2021.123316

[13] Li, Y., Shi, T., Li, J. "Effects of fly ash and quartz sand on water-resistance and salt-resistance of magnesium phosphate cement", Construction and Building Materials, 105, pp. 384–390, 2016. https://doi.org/10.1016/j.conbuildmat.2015.12.154

[14] Li, G., Zhang, J., Zhang, G. "Mechanical property and water stability of the novel CSA-MKPC blended system", Construction and Building Materials, 136, pp. 99–107, 2017. https://doi.org/10.1016/j.conbuildmat.2017.01.036

[15] Zhong, D., Wang, S., Wang, L. "The influence of alkaline curing systems on the strength and microstructural properties of magnesium phosphate cement", Construction and Building Materials, 264, 120679, 2020. https://doi.org/10.1016/j.conbuildmat.2020.120679

[16] You, C., Qian, J., Qin, J., Wang, H., Wang, Q., Ye, Z. "Effect of early hydration temperature on hydration product and strength development of magnesium phosphate cement (MPC)", Cement and Concrete Research, 78, pp. 179–189, 2015. https://doi.org/10.1016/j.cemconres.2015.07.005

[17] Xu, B., Winnefeld, F., Lothenbach, B. "Effect of temperature curing on properties and hydration of wollastonite blended magnesium potassium phosphate cements", Cement and Concrete Research, 142, 106370, 2021. https://doi.org/10.1016/j.cemconres.2021.106370

[18] Sarkar, A. K. "Hydration/dehydration characteristics of struvite and dittmarite pertaining to magnesium ammonium phosphate cement systems", Journal of Materials Science, 26, pp. 2514–2518, 1991. https://doi.org/10.1007/BF01130204

[19] Qin, J., Qian, J., You, C., Fan, Y., Li, Z., Wang, H. "Bond behavior and interfacial micro-characteristics of magnesium phosphate cement onto old concrete substrate", Construction and Building Materials, 167, pp. 166–176, 2018. https://doi.org/10.1016/j.conbuildmat.2018.02.018

[20] Park, J. W., Kim, K. H., Ann, K. Y. "Fundamental Properties of Magnesium Phosphate Cement Mortar for Rapid Repair of Concrete", Advances in Materials Science and Engineering, 2016(1), 7179403, 2016. https://doi.org/10.1155/2016/7179403

[21] Morgan, D. R. "Compatibility of concrete repair materials and systems", Construction and Building Materials, 10(1), pp. 57–67, 1996. https://doi.org/10.1016/0950-0618(95)00060-7

[22] Li, J., Zhang, W., Cao, Y. "Laboratory evaluation of magnesium phosphate cement paste and mortar for rapid repair of cement concrete pavement", Construction and Building Materials, 58, pp. 122–128, 2014. https://doi.org/10.1016/j.conbuildmat.2014.02.015

[23] Yang, Q., Zhu, B., Zhang, S., Wu, X. "Properties and applications of magnesia–phosphate cement mortar for rapid repair of concrete", Cement and Concrete Research, 30(11), pp. 1807–1813, 2000. https://doi.org/10.1016/S0008-8846(00)00419-1

[24] Haque, M. A., Chen, B., Li, S. "Water-resisting performances and mechanisms of magnesium phosphate cement mortars comprising with fly-ash and silica fume", Journal of Cleaner Production, 369, 133347, 2022. https://doi.org/10.1016/j.jclepro.2022.133347

[25] Fan, S., Chen, B. "Experimental research of water stability of magnesium alumina phosphate cements mortar", Construction and Building Materials, 94, pp. 164–171, 2015. https://doi.org/10.1016/j.conbuildmat.2015.06.050

[26] Feng, H., Lv, L., Pang, Y., Yuan, C., Chu, L., Zhao, X. "Bond behavior between the nano-Al_2O_3-water-glass-modified magnesium-phosphate-cement mortar and steel fiber", Construction and Building Materials, 306, 124814, 2021. https://doi.org/10.1016/j.conbuildmat.2021.124814

[27] Qin, J., Dai, F., Ma, H., Dai, X., Li, Z., Jia, X., Qian, J. "Development and characterization of magnesium phosphate cement based ultra-high performance concrete", Composites Part B: Engineering, 234, 109694, 2022. https://doi.org/10.1016/j.compositesb.2022.109694

[28] Gadekar, S., Pullammanappallil, P. "Validation and Applications of a Chemical Equilibrium Model for Struvite Precipitation", Environmental Modeling and Assessment, 15(3), pp. 201–209, 2010. https://doi.org/10.1007/s10666-009-9193-7

[29] de Vargas, A. S., Dal Molin, D. C. C., Masuero, Â. B., Vilela, A. C. F., Castro-Gomes, J., de Gutierrez, R. M. "Strength development of alkali-activated fly ash produced with combined NaOH and $Ca(OH)_2$ activators", Cement and Concrete Composites, 53, pp. 341–349, 2014. https://doi.org/10.1016/j.cemconcomp.2014.06.012

[30] Zhu, X., Tang, D., Yang, K., Zhang, Z., Li, Q., Pan, Q., Yang, C. "Effect of $Ca(OH)_2$ on shrinkage characteristics and microstructures of alkali-activated slag concrete", Construction and Building Materials, 175, pp. 467–482, 2018. https://doi.org/10.1016/j.conbuildmat.2018.04.180

[31] Jia, Z., Chen, C., Shi, J., Zhang, Y., Sun, Z., Zhang, P. "The microstructural change of C-S-H at elevated temperature in Portland cement/GGBFS blended system", Cement and Concrete Research, 123, 105773, 2019. https://doi.org/10.1016/j.cemconres.2019.05.018

[32] Bahafid, S., Ghabezloo, S., Duc, M., Faure, P., Sulem, J. "Effect of the hydration temperature on the microstructure of Class G cement: C-S-H composition and density", Cement and Concrete Research, 95, pp. 270–281, 2017. https://doi.org/10.1016/j.cemconres.2017.02.008

[33] Wang, J., Xu, L., Ma, L., He, H., Wang, Y., Xiang, D., Lin, S., Zhong, Y., Zhao, H. "Effect of pre-carbonation on the properties of cement paste subjected to high temperatures", Journal of Building Engineering, 51, 104337, 2022. https://doi.org/10.1016/j.jobe.2022.104337

[34] Collepardi, M. "A state-of-the-art review on delayed ettringite attack on concrete", Cement and Concrete Composites, 25(4–5), pp. 401–407, 2003. https://doi.org/10.1016/S0958-9465(02)00080-X

[35] Zhang, S., Li, Q., Yuan, Q., Yang, S., Dai, X. "Effect of roughness on bonding performance between Portland cement concrete and magnesium phosphate cement concrete", Construction and Building Materials, 323, 126585, 2022. https://doi.org/10.1016/j.conbuildmat.2022.126585

[36] Le Rouzic, M., Chaussadent, T., Stefan, L., Saillio, M. "On the influence of Mg/P ratio on the properties and durability of magnesium potassium phosphate cement pastes", Cement and Concrete Research, 96, pp. 27–41, 2017. https://doi.org/10.1016/j.cemconres.2017.02.033

[37] Lv, L., Huang, P., Mo, L., Deng, M., Qian, J., Wang, A. "Properties of magnesium potassium phosphate cement pastes exposed to water curing: A comparison study on the influences of fly ash and metakaolin", Construction and Building Materials, 203, pp. 589–600, 2019. https://doi.org/10.1016/j.conbuildmat.2019.01.134

[38] Chong, L., Yang, J., Shi, C. "Effect of curing regime on water resistance of magnesium–potassium phosphate cement", Construction and Building Materials, 151, pp. 43–51, 2017. https://doi.org/10.1016/j.conbuildmat.2017.06.056

[39] Li, Y., Li, Z., Pei, H., Yu, H. "The influence of $FeSO_4$ and KH_2PO_4 on the performance of magnesium oxychloride cement", Construction and Building Materials, 102, pp. 233–238, 2016. https://doi.org/10.1016/j.conbuildmat.2015.10.186

[40] Li, Y., Shi, T., Chen, B., Li, Y. "Performance of magnesium phosphate cement at elevated temperatures", Construction and Building Materials, 91, pp. 126–132, 2015. https://doi.org/10.1016/j.conbuildmat.2015.05.055

[41] Qoku, E., Scheibel, M., Bier, T., Gerz, A. "Phase development of different magnesium phosphate cements at room temperature and elevated temperatures", Construction and Building Materials, 272, 121654, 2021. https://doi.org/10.1016/j.conbuildmat.2020.121654

[42] Ruan, W., Li, F., Liao, J., Gu, X., Mo, J., Shen, Y., Zhu, Y., Ma, X. "Effects of water purifying material waste on properties and hydration mechanism of magnesium phosphate cement-based grouting materials", Construction and Building Materials, 349, 128676, 2022. https://doi.org/10.1016/j.conbuildmat.2022.128676

[43] Haque, M. A., Chen, B. "Research progresses on magnesium phosphate cement: A review", Construction and Building Materials, 211, pp. 885–898, 2019. https://doi.org/10.1016/j.conbuildmat.2019.03.304

[44] Chau, C. K., Qiao, F., Li, Z. "Microstructure of magnesium potassium phosphate cement", Construction and Building Materials, 25(6), pp. 2911–2917, 2011. https://doi.org/10.1016/j.conbuildmat.2010.12.035

[45] Gardner, L. J., Bernal, S. A., Walling, S. A., Corkhill, C. L., Provis, J. L., Hyatt, N. C. "Characterisation of magnesium potassium phosphate cements blended with fly ash and ground granulated blast furnace slag", Cement and Concrete Research, 74, pp. 78–87, 2015. https://doi.org/10.1016/j.cemconres.2015.01.015

[46] Jia, L., Zhao, F., Yao, K., Du, H. "Bond performance of repair mortar made with magnesium phosphate cement and ferroaluminate cement", Construction and Building Materials, 279, 122398, 2021. https://doi.org/10.1016/j.conbuildmat.2021.122398

[47] Li, L., Wang, Q., Zhang, G., Shi, L., Dong, J., Jia, P. "A method of detecting the cracks of concrete undergo high-temperature", Construction and Building Materials, 162, pp. 345–358, 2018. https://doi.org/10.1016/j.conbuildmat.2017.12.010